Hindawi
Journal of Nanotechnology
Volume 2023, Article ID 5381158, 8 pages
https://doi.org/10.1155/2023/5381158

Research Article

Size and Morphology-Mediated Antiproliferative Activity of Hydroxyapatite Nanoparticles in Human Breast Cancer Cells

Moeko Fukada,[1] Tilak Chhetri,[2,3] Agasthya Suresh,[2,3] Anandhi Upendran,[2,4,5] and Zahra Afrasiabi[1]

[1]*Life Sciences, Soka University of America, Aliso Viejo, CA, USA*
[2]*Department of Chemical and Biomedical Engineering, University of Missouri, Columbia, MO, USA*
[3]*Department of Radiology, University of Missouri, Columbia, MO, USA*
[4]*Department of Medical Pharmacology and Physiology, University of Missouri, Columbia, MO, USA*
[5]*Institute of Clinical and Translational Sciences (MU-iCATS), School of Medicine, University of Missouri, Columbia, MO, USA*

Correspondence should be addressed to Zahra Afrasiabi; zafrasiabi@soka.edu

Received 4 October 2022; Revised 27 February 2023; Accepted 9 March 2023; Published 18 April 2023

Academic Editor: Sekar Vijayakumar

Hydroxyapatite nanoparticles (nHAPs) have been recognized for potent antitumor effects in certain cancer cells, making them good candidates as drug delivery agents and tumor therapeutics with fewer than normal side effects. This study is aimed to correlate cell proliferation inhibition with the size and morphology of nHAPs in a human breast cancer cell line as well as in normal tissue cells. We present our in vitro experimental evidence that nHAPs with sizes smaller than 50 nm have high inhibitory activity against human MCF-7 breast cancer cell lines. Based on our experimental data, normal fibroblast cells (NIH 3T3) were relatively more viable upon treatment with the nanoconstructs. The present study indicates that nHAPs can be engineered as nontoxic specific inhibitors as efficient breast cancer therapeutics in humans.

1. Introduction

Due to the nature of traditional chemotherapy, which is the leading method for controlling tumor growth, certain normal tissues also get damaged while inhibiting tumor cell growth. This leads to severe side effects in patients receiving chemotherapeutic drugs [1–3]. Common side effects of cancer chemotherapy can be acute or prolonged including hypersensitivity reactions to infusion, nausea and vomiting, mucositis, fatigue, diarrhea, constipation, and neurotoxicity [4].

Therefore, chemotherapeutic drugs that can cause minimal side effects have attracted tremendous research attention seeking to alleviate patient pain. Across the world, breast cancer is still among the deadliest cancer and is responsible for countless deaths [5]. Thus, there is a pressing demand to develop more efficient and safer agents that can control breast cancer aggression and inhibit cancer cell proliferation.

Hydroxyapatite [HAP, $Ca_{10}(PO_4)_6(OH)_2$], a calcium-based biomaterial, has been employed widely in orthopedic and dental applications [6]. Being the principal inorganic constituent of human bones and teeth, HAP has shown excellent biocompatibility, bioactivity, and bone-bonding properties. It is also used as a vehicle for drug, protein, and gene delivery [7].

Nanodimensional HAP is the main mineral component of natural bone. HAP in natural bone is in nanosized needle-shaped crystal form (5–20 nm width and 60 nm length) and present in collagen fiber matrix with poorly crystallized nonstoichiometric apatite phase containing CO_3^{2-}, Na^+, F^-, and other ions [8]. Despite HAP's similar composition to the mineral component of bone, major challenges have been encountered due to lack of its mechanical and antimicrobial properties, low degradation, targeted deficiency, and lesser drug loading capability. One of the approaches to improve the performance of synthetic HAP is synthesizing these particles to nanodimensional size, which results in a larger

surface area to volume-ratio and emergence of quantum effects [9]. Compared with the macro size formulations, nanosized HAP particles exhibit properties, such as grain size, pore size, and surface area, wettability, which influence protein interactions in the form of bioactivity, adsorption, configuration, and improve mechanical properties, sinterability, and higher drug loading and favorably release characteristics [10–14].

Researchers have been investigating the antiproliferation capability of hydroxyapatite nanoparticles (nHAPs) and their application as delivery vehicles for growth factors [15], antibiotics [16], antiangiogenesis drugs [17], enzymes [18], and antigens for slow-release vaccination [19]. These nHAP particles have been found to be capable of inhibiting proliferation and inducing apoptosis in various cancer cells, including osteosarcoma cells [20], breast cancer cells [17, 21, 22], gastric cancer cells [23, 24], colon cancer cells [25], and liver cancer cells [26, 27].

Remarkably, it has been shown that when the nHAP particle diameter is less than 100 nm, it has a substantially higher inhibitory effect on the metabolic viability of tumor cells when compared to conventional biocompatibility [28, 29]. In general, the nanoparticles' morphology- and size-dependent cytotoxicity, cellular uptake, and bioactivity are directly related to the synthesis methods applied to prepare these materials [20, 30].

The correlation between the size and morphology of nHAP particles and their antiproliferative effect on breast cancer cells has not been studied previously. In this study, we have synthesized nHAPs of various sizes and morphologies using different synthetic methods and have explored their inhibitory effect on the growth of MCF-7 human breast cancer cells and normal cells (NIH 3T3). The nHAPs were synthesized by chemical precipitation, hydrolysis, and hydrothermal methods and characterized by transmission electron microscopy (TEM), X-ray diffraction (XRD), and Fourier-transform infrared (FT-IR) spectroscopy. Cell viability was detected with an MTT colorimetric assay on the human breast cancer cell line (MCF-7) and mouse fibroblast cell line (NIH 3T3).

2. Materials and Methods

2.1. Materials. Calcium nitrate, ammonium solution (30%), ethyl alcohol (pure), sodium hydroxide (purity 95%), calcium hydrogen phosphate dehydrate (DCPD) (purity ≥ 98%), potassium phosphate dibasic trihydrate (99.0%), potassium hydroxide, calcium chloride, oleic acid (≥99%), calcium stearate, and trisodium phosphate were purchased from Sigma-Aldrich. Hexadecyltrimethylammonium bromide (CTAB) (purity 96.6%) and ethylenediamine (85 wt%) were purchased from Merck. Phosphoric acid (85%) and toluene were purchased from Fisher Scientific. Sodium citrate dihydrate was purchased from Spectrum. Ultrapure water (Millipore, 18.2 MΩ·cm) was used to prepare all solutions. RPMI1640 media was purchased from ATCC (30–2001). Fetal bovine serum was purchased from Sigma (F0926). Stock suspensions were (bath) sonicated for 60 sec before preparing dilutions in serum-containing media. The CellTiter 96® Nonradioactive Cell Proliferation Assay was purchased from Promega (G4000).

2.2. Instrumentation. The nHAPs were analyzed by Fourier-transform infrared spectroscopy (FT-IR, Perkin-Elmer Spectrum Two ATR, 400–4000 cm^{-1}). X-ray diffraction (XRD) experiments were performed at room temperature on a Rigaku SmartLab diffractometer equipped with a high-accuracy/resolution four-circle theta-theta goniometer, using Cu Kα radiation and a Dtex Ultra detector with a scan range of $2\theta = 20^{\circ}$–80°, a scanning rate of 1°/min, a voltage of 40 kV, and a current of 44 mA. Zeta potential of the nHAP particles was determined in phosphate buffered solution (PBS) with pH 7.4 using a Zetasizer Nano S90 (Malvern Instruments Ltd. USA) in folded capillary cells. Transmission electron microscope (TEM) images were obtained on a JEOL JEM-1400 120 kV transmission electron microscope (Japan). The samples were prepared by placing 5 μL of 0.1 mg/ml nanoparticle solution on the CF300-Cu carbon film-based copper grid, and the solution was allowed to settle for 5 min. The grid was then air-dried for an additional 5 min. The average size and the size distribution of the nanoparticles were determined by processing the TEM images with image processing software (Adobe Photoshop with Fovea plug-ins). The core size of the nanoparticles was also measured on a DC 24000, CPS Instruments Inc. (USA).

2.3. Synthesis of nHAPs. The nHAP particles were synthesized using three reported wet methods with slight modifications: hydrolysis method (nHAP-1) [31], hydrothermal method (nHAP-2, nHAP-4) [32, 33], and chemical precipitation (nHAP-3) [34].

2.3.1. Synthesis of nHAP-1. First, 20 g (500 mmol) of NaOH was dissolved in a mixture of 60 mL of deionized water and 140 mL of ethanol and heated to 75°C. Then, 0.0364 g (0.1 mmol) of CTAB was added and stirred until the solution was clear. Subsequently, 1.3 g (10 mmol) of DCPD was added to the solution and mixed at 75°C for 1 h. After homogenization, the solution was cooled in an ice bath for 20 min to allow precipitation to occur. The precipitates were filtered by vacuum filtration and rinsed with deionized water three times. The resulting powder was oven-dried at 60°C overnight.

2.3.2. Synthesis of nHAP-2. First, 250 mL of 0.1 M $CaCl_2$ solution was added to 250 mL of 0.06 M KH_2PO_4 solution using a syringe pump (Chemyx Fusion 200) with a flow rate of 125 mL/hr and stirred. The pH of the reaction mixture was increased from 4.00 to 8.00 by the dropwise addition of ethylenediamine using a pH meter (VWR Symphony B40PCID). The resultant suspension was transferred to a Teflon™-lined autoclave and kept in the oven at 180°C for 12 h. The precipitates were centrifuged at 3500 rpm (Thermo Sorvall ST 8R) and washed with anhydrous ethanol and deionized water prior to oven-drying at 80°C for 12 h.

2.3.3. Synthesis of nHAP-3. First, 100 mL of 0.6 M phosphoric acid and 100 mL of 1 M calcium nitrate tetrahydrate aqueous solutions (ratio Ca/P 1.67, characteristic of calcium hydroxyapatite) were mixed at 40°C in a water bath, followed by the addition of 5 mL of (0.34 M) sodium citrate dihydrate aqueous solution. The pH of the reaction mixture was increased from 0.9 to 10 by adding ammonia solution (30%) dropwise. The resultant solution was allowed to react for an additional 8 h at 40°C in the water bath and was then transferred into a Teflon™-lined autoclave and heated at 100°C for 8 h. Finally, the resultant cloudy solution was centrifuged at 4500 rpm, and precipitates were washed with deionized water until they reached a pH of 7, after which they were oven-dried at 100°C overnight.

2.3.4. Synthesis of nHAP-4. First, 0.548 g (2.4 mmol) K_2HPO_4 $3H_2O$ and 1.64 g (4.5 mmol) of CTAB were added to 100 mL degasified water prepared using a vacuum pump and a filtering flask. After incubation of the solution at 50°C for 2 h, the pH was increased from 9 to 12 by adding 4 mL of KOH using a pH meter. Using the syringe pump, 60 mL of 0.33 M $CaCl_2$ solution was added under gentle magnetic stirring with a flow rate of 20 mL/h. The solution was covered with aluminum foil and heated in the oven at 120°C for 12 h. The produced precipitate was washed with degasified water and ethanol by centrifugation at 4500 rpm and again at 2500 rpm. The precipitate was isolated and oven-dried at 90°C for 24 h.

2.4. Cell Viability Assay (MTT). The nanoconstructs (nHAPs 1–4) were ground using a mortar and pestle, and stock suspensions at 1 mg/mL were prepared using RPMI1640 media containing 10% fetal bovine serum (FBS). Stock suspensions were (bath) sonicated (Fisherbrand CPX2800 bath sonicator, 40 KHz, 110 Watts, 2.5 L) and vortexed, comprising of 4 rounds of 15 seconds sonication and 5 seconds vortex, to form a homogenous solution before preparing dilutions in serum-containing media. Human breast cancer cells (MCF-7) and mouse fibroblast cells (NIH 3T3) were seeded in 96 well plates (MCF-7: 3000 cells per well and NIH 3T3: 4500 cells per well) using the Integra Assist Plus automated pipettor. Following overnight incubation at 37°, 5% CO_2, the cells were washed and incubated with seven concentrations of each construct in the range of 200 μg/mL to 20 μg/mL dry weight for 72 h at 37°C; 5% CO_2. A CellTiter 96® Nonradioactive Cell Proliferation Assay was used to analyze the cell viability per the manufacturer's instructions. A nonlinear regression curve (Absolute IC50 equation; GraphPad Prism 8.4.2) was used to calculate the dry weight IC50 for each construct.

3. Results and Discussion

Previous reports have clearly demonstrated that the antitumor effect of nHAPs might be related to their inherent physicochemical characteristics, including their morphology and crystal size. In this study, to synthesize nHAPs with different morphology and size, hydrolysis, hydrothermal, and chemical precipitation methods were applied. Most nHAP products have long rod- or needle-like morphology because of their hexagonal crystalline structures. However, by aiming toward the synthesis of smaller crystallite size particles, the shape of the nanoconstructs can be shorter and rounder with a larger surface area [31]. Hydrothermal synthesis is the easiest and most effective method to obtain crystalline and well dispersed nHAPs. Proceeding with the hydrothermal method under high temperature and pressure improved the reactivity because the reaction process and the mechanism were relatively different from what is typically employed. The product had high purity, good dispersibility, and a rod-shaped morphology (nHAP-2, 32% yield, and 100 nm in length). To modify the morphology and obtain smaller-sized nanocrystals using the hydrothermal method, a calcium source was added using a controlled dripping flow rate in the presence of organic additives (nHAP-4, 2.56% yield, and 40–50 nm hexagonal). The chemical precipitation method from an aqueous solution containing an organic modifier yielded well-defined hexagonal nanorods (nHAP-3, 43% yield, and 100–300 nm in length) at low temperature. To obtain a small-sized, sphere-like nanostructure rather than a rod-like shape, the hydrolysis method in the presence of alcohol was used (nHAP-1, 80% yield, 10 nm in diameter).

X-ray diffraction (XRD) analysis was performed to determine the crystalline structure of the synthesized hydroxyapatite nanoparticles (Figure 1). HAP's crystal structure is characterized by the space group $P6_3/m$, which has a *c*-plane with negative charge due to its rich content of PO_4^{3-} ions and a positively charged *a*-plane due to its high content of Ca^{2+} ions [35]. In the case of the crystal orientations, the *a*, *b*-plane and *c*-plane have different functions, as they are seen in response in different parts of the body. For example, the *a*, *b*-plane is bioactive for human saliva and bioinert for the surface of human teeth. For this reason, an HAP surface with *a*, *b*-plane would be suitable in a bone filler [36].

All samples showed the characteristic peaks of the hydroxyapatite structure by comparing the obtained experimental XRD patterns to the standards complied by the International Centre for Diffraction Data (ICDD) for hexagonal crystal structures (JCPDS, No: 09–0432). The hexagonal form of HAP is more stable than its monoclinic structure and is found in most biological apatite but in nonstoichiometric composition [37]. Needle- or rod-shaped morphology is preferred oriented growth of HAP since its unit cells are structured along the *c*-axis. The characteristic peak of the highest intensity for nHAPs 1–4 was obtained at 2θ values of 31.92°, 31.78°, 31.56°, and 31.56°, corresponding to the (2 1 1) plane, respectively. A broadening line and a decrease in intensity were observed in the XRD pattern of nHAP-1, indicating that the crystallinity of nHAP-1 was lower than that of the other three nanoparticle samples, and it exhibited sharp characteristic peaks at corresponding planes for hydroxyapatite. The broad reflection peaks on the XRD patterns in the region between 20° and 50° 2θ are usually characteristic of either partially amorphous or nanoparticulate material [38].

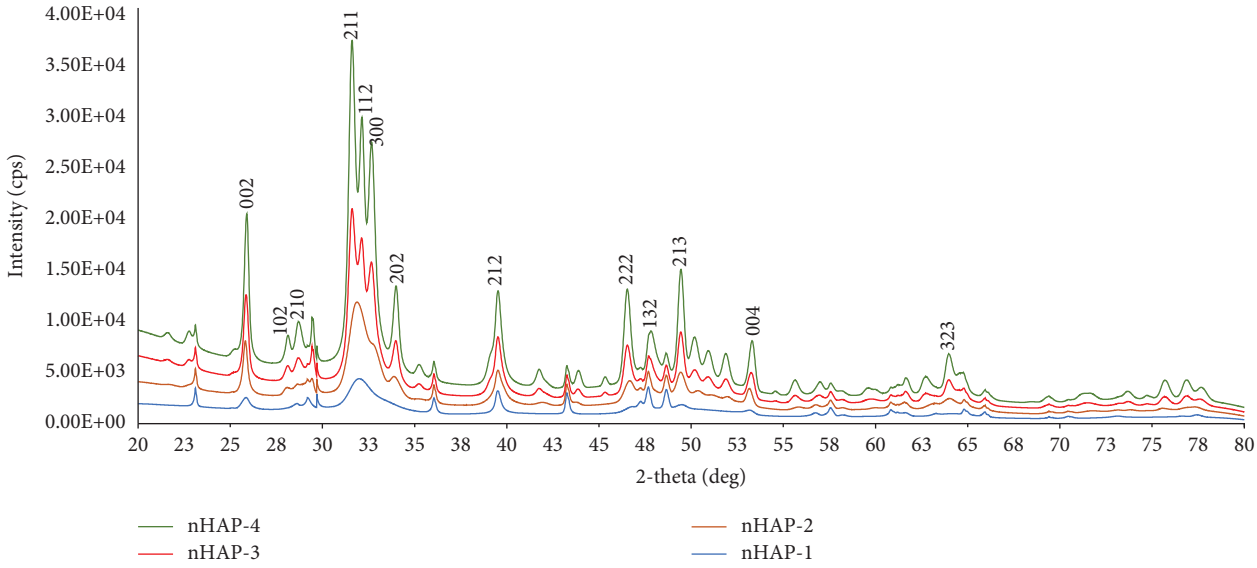

Figure 1: XRD diffractograms of hydroxyapatite nanoparticles (nHAPs 1–4).

As depicted in Figure 2, the TEM morphology of the nHAP-1 nanoparticles showed a spherical shape with a diameter of about 10 nm. The nHAP-2 nanoparticles were in the form of rods and uniformly distributed, with an average size of 100 nm (length) × 30 nm (width). The nHAP-3 nanoparticles were observed as rod-like shapes with a size range of 100–300 nm (length) × 20 nm (width), while the nHAP-4 particles were found to be 40–50 nm with hexagonal shape.

nHAPs 1–4 all showed negative zeta potentials, -2.31 ± 0.65 mV, -3.9 ± 0.83 mV, -10.72 ± 0.74 mV, and 5.30 ± 0.86 mV, respectively, in PBS solution at pH 7.4. The recorded values are consistent with previous studies by other researchers [39–41]. Tang et al. reported that the zeta potential of HAP nanoparticles become more negative as the size increases; and the zeta potential of HAP nanoparticles with size of 20 nm, 40 nm, and 80 nm are -4.1 ± 0.6 mV, -4.8 ± 0.2 mV, and -6.0 ± 1.0 mV, respectively [42]. As depicted in TEM images, the length of the nHAP-3 nanoparticle is larger than 100 nm, which is probably the reason for its more negative zeta potential value. Correspondingly, Chen et al. reported -11.7 ± 0.7 mV as the zeta potential value of nanoparticles with the length of 150 nm [43]. Surfactants are often used to overcome the issue of aggregation when synthesizing nanomaterials. Surface modification by the cationic surfactant, cetyltrimethyl ammonium bromide (CTAB) that contains quaternary ammonium salt, provides more positive sites on the surface of the nHAP-1 and nHAP-4 and results in more positive zeta potential [44]. The concentration of CTAB used for preparation of nHAP-4 was higher compared to the amount used in nHAP-1 synthesis; hence, the positive increase in zeta potential value is more reflected in the nHAP-4 particle.

Fourier-transform infrared (FT-IR) characterization was recorded for each sample to verify the spectral characteristics indicative of chemical bonding. The bending mode of the O\\P\\O chemical bonds was observed at 467, 472, 473, and 472 cm^{-1} for nHAPs 1–4, respectively. The peak at 633 cm^{-1} due to the apatite hydroxyl symmetric mode was identified in the spectra of nHAPs 1–3, whereas for nHAP-1, this band was combined with the phosphate fundamental modes around 600 cm^{-1}. Phosphate fundamental modes with two sharp intense peaks in the 560 to 602 cm^{-1} region and one small band in the 600 to 635 cm^{-1} region were present for all of the nano-apatites. The phosphate symmetric stretching mode ($\upsilon 1$) from 959 to 962 cm^{-1} and the sharp intense phosphate asymmetric stretching modes ($\upsilon 3$) between 1022 and 1091 cm^{-1} were identified in all samples. The small bands around 3570 cm^{-1} were associated with–OH stretching vibrations in the HAP nanomaterials.

The in vitro cytotoxicity of the four nanoconstructs was investigated in breast cancer cells (MCF-7) and normal fibroblast cells (NIH 3T3) in a concentration range from 20 to 200 μg/mL. The nanoconstructs exhibited cytotoxicity on the breast cancer cells, while the normal cells were relatively less affected (absolute IC50 >> 200 μg/mL). Both nHAP-1 and nHAP-4 were significantly more cytotoxic compared to nHAP-2 and nHAP-3. The absolute IC50 values of nHAP-4 and nHAP-1 were ~16 μg/mL and ~29.7 μg/mL, respectively (Figure 3). NIH 3T3 cells were relatively more viable upon treatment with the nanoconstructs (Figure 4). The long rod-like nanoconstructs (nHAP-2 and nHAP-3) had less inhibitory effect on the cell proliferation of the MCF-7 cells compared to the small spherical and hexagonal nanoparticles (nHAP-1 and nHAP-4). By varying the conventional rod- or needle-like growth habit of the nHAPs and developing sphere-like particles, Zhao et al. also presented evidence that spherical nHAPs have high inhibitory activity against mouse 4T1 cell lines [45].

Different concentrations of nHAP-1, having the smallest size among the four synthesized nanoparticles and with a spheric shape, had different toxicities on the MCF-7 cells. The higher the nHAP-1 concentration, between 20 and 200 μg/mL, the stronger the toxicity. However, the dose-

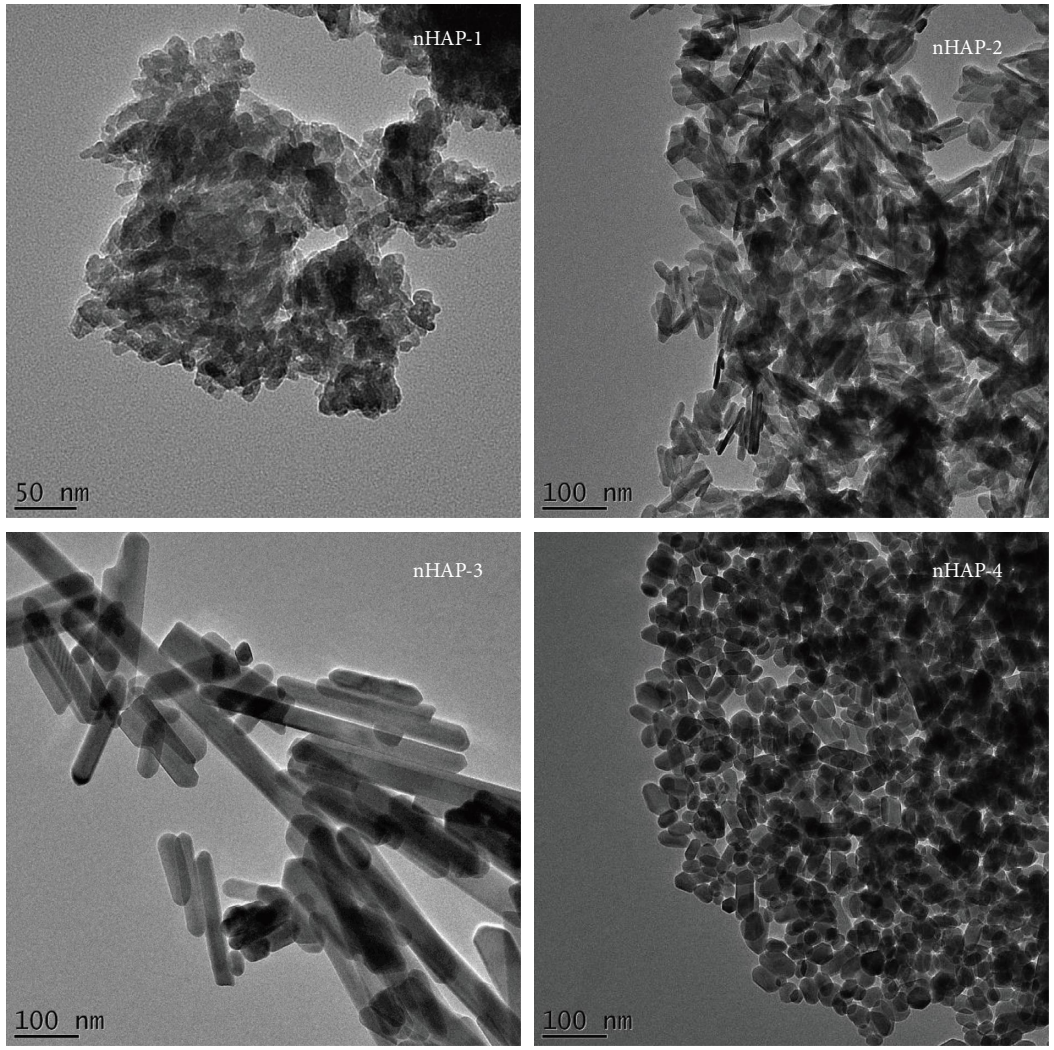

Figure 2: TEM images of nHAP nanoparticles.

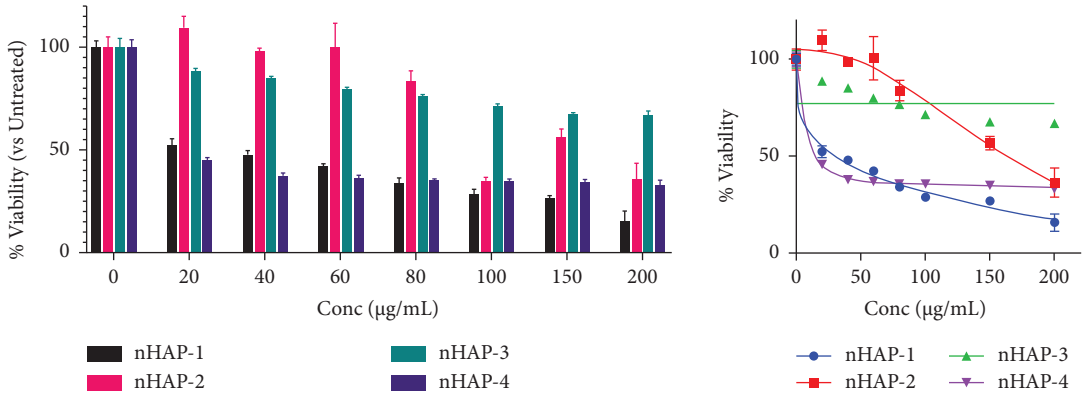

Figure 3: In vitro cytotoxicity of nHAP constructs in MCF-7 breast cancer cells.

dependency of the toxicity of the nHAP-4 to the MCF-7 cells was not significant.

Unlike inducing cell multiplication and differentiation of nHAP when used for bone construction, apoptosis stimulation and decrease in cell proliferation are observed once applied in tumor therapies [46]. Our results are consistent with previously reported results by Yuan et al. in which they have demonstrated the size dependency apoptosis of nHAP [30]. The antitumor activity and nHAP-induced apoptosis on human hepatoma HepG2 cells strongly depended on the size of the nanoparticles, and the cytotoxic effects decreased upon increasing the size from 20 to 175 nm.

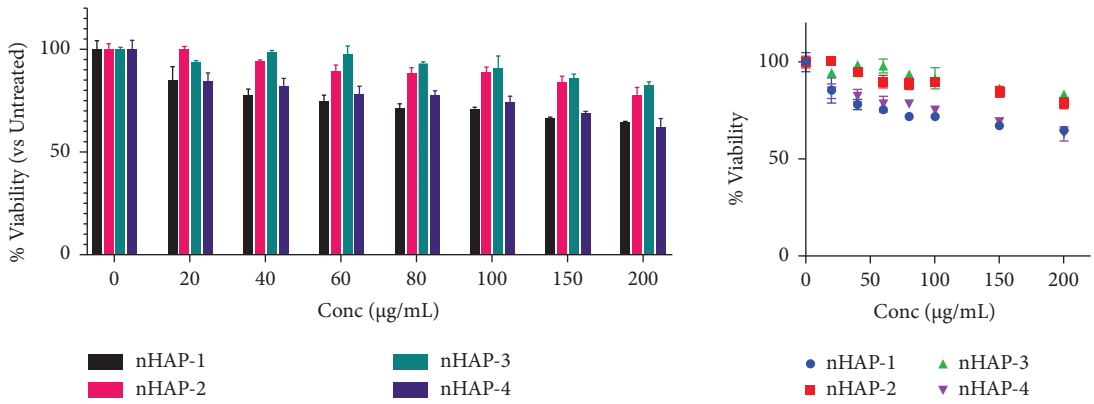

Figure 4: In vitro cytotoxicity of nHAP constructs in NIH 3T3 fibroblast cells.

nHAP functionalities to a great extent depend on the adhesion process and cellular internalization, which are reported to be greatly influenced by nanoparticle size [47, 48]. Two distinct routes to get into the cells are proposed for nHAP internalization: endocytosis and phagocytosis [49]. In the first method, they cross the cell membrane and spread freely through the cytosol and get into organelles and nucleus. Phagocytosis is the second rout, in which cells' pseudopods engulf nHAP, which are retained in endosomes, followed by transportation to lysosomes, and finally dissolved within the vesicle [49]. Recurrent reported result has mentioned that the extent of internalization is inversely proportional to the size of the nanoparticle [47–49].

The pathways for programmed death mechanisms activation rely on the adsorption and internalization of the nanoparticles in cancer cells [47, 50]. Apoptosis was also observed when umbilical cord endothelial cells and renal epithelial cells were treated with nHAP [51–53]. nHAPs in lysosomes generated reactive oxygen species that activated a programmed cell death as an apoptosis mechanism in the studied cancer cells [52–54]. In another study, Gua et al. reported that nHAPs blocked the signaling pathway of nuclear factors (NF-kb) by generation of free radicals in Glioma cells, resulted in apoptosis or cell cycle arrest in G2/M phases and therefore reduced the proliferative capacity of the tumor [46]. In a systematic assessment of nHAPs used in the treatment of Melanoma, it was concluded that cancerous cells capture high concentrations of nHAPs due to the enhanced permeability and retention (EPR) effect, which increases free radical synthesis by cell organelles and leads to the cell death [55, 56]. Zhao et al. evaluated the antitumor properties of hydroxyapatite nanospheres both in vitro on the 4T1 murine mammary carcinoma cell line and in vivo on the 4T1 xenograft model. The hydroxyapatite nanospheres were found to be highly compatible with normal tissues but also had excellent antitumor activities. Systematic investigation on the mechanism of apoptosis induced by hydroxyapatite nanospheres on tumor cells confirmed the ingrained mitochondria-dependent apoptosis pathway accompanied by negative regulation of the PIK3/AKT pathway [45].

Similar to the present study, Tang et al. observed selective toxicity of nHAP with lower toxicity on liver cell line (L-02) compared to gastric cancer cells (MGC80-3), cervical adenocarcinoma (HeLa) cells, and hepatocarcinoma (HepG2) cells. Neoplastic cells when compared to normal cells present electrolyte and metabolic imbalance that result in different intracellular localization. The unregulated intracellular ionic variation makes the cancer cells to internalize large concentrations of nanoparticles and subsequently disposes them to more damage when treated with nanoparticles [57].

4. Conclusion

The well-researched application for nHAP has been in the reconstruction of bone tissues; however, the present work is focused on studying the aspect of the antiproliferative capability of these nanoparticles when evaluated for cancer treatment. The existing data relates the antiproliferative activity of nHAPs to their ability of inducing cellular apoptosis as a consequence of their higher internalized concentration. Particles with smaller sizes and more compact structures are more easily internalized in the cells. Our study validates that reshaping the inherent growth habit of nHAPs by applying modified synthetic procedures can lead to the formation of sphere-like nHAPs with sizes of approximately 50 nm and under. Most notably, nHAPs displayed unique size-dependent cytotoxicity on breast cancer cells making them a highly promising choice for tumor therapy to avoid the agonizing effects associated with the administration of traditional chemotherapy drugs. Further studies are necessary to examine the cell proliferation inhibition mechanism induced by nHAPs in breast cancer cells correlated with modulating the inhibitory effect of the particle size and morphology.

Data Availability

Data used to support the findings of this study are included within the manuscript.

Conflicts of Interest

The authors declare that they have no conflicts of interest.

Acknowledgments

The authors appreciate the financial support from Soka University's Presidential Research Funding Program.

References

[1] D. Weycker, A. Silvia, K. Richert-Boe et al., "Use and patterns of supportive care among patients receiving myelosuppressive chemotherapy for breast cancer, colorectal cancer, lung cancer, or non-hodgkin's lymphoma in US clinical practice," *Blood*, vol. 128, no. 22, p. 5909, 2016.

[2] J. Herrstedt, S. Lindberg, and P.-C. Petersen, "Prevention of chemotherapy-induced nausea and vomiting in the older patient: optimizing outcomes," *Drugs and Aging*, vol. 39, pp. 1–21, 2022.

[3] J.-Y. Kim, J. Ohn, J.-S. Yoon et al., "Priming mobilization of hair follicle stem cells triggers permanent loss of regeneration after alkylating chemotherapy," *Nature Communications*, vol. 10, no. 1, p. 3694, 2019.

[4] M. T. Amjad, A. Chidharla, and A. Kasi, "Cancer chemotherapy," in *StatPearls*, StatPearls Publishing, Treasure Island, FL, USA, 2022.

[5] R.-L. Siegel, K.-D. Miller, and A. Jemal, "Cancer statistics, 2019," *CA: A Cancer Journal for Clinicians*, vol. 69, no. 1, pp. 7–34, 2019.

[6] K. Zhang, Y. Zhou, C. Xiao et al., "Application of hydroxyapatite nanoparticles in tumor-associated bone segmental defect," *Science Advances*, vol. 5, no. 8, Article ID eaax6946, 2019.

[7] Z. Tang, X. Li, Y. Tan, H. Fan, and X. Zhang, "The material and biological characteristics of osteoinductive calcium phosphate ceramics," *Regenerative Biomaterials*, vol. 5, no. 1, pp. 43–59, 2018.

[8] M. P. Ferraz, F. J. Monteiro, and C. M. Manuel, "Hydroxyapatite nanoparticles: a review of preparation methodologies," *Journal of Applied Biomaterials and Biomechanics: JABB*, vol. 2, no. 2, pp. 74–80, 2004.

[9] G. Singh, R. P. Singh, and S. S. Jolly, "Customized hydroxyapatites for bone-tissue engineering and drug delivery applications: a review," *Journal of Sol-Gel Science and Technology*, vol. 94, no. 3, pp. 505–530, 2020.

[10] T. J. Webster, C. Ergun, R. H. Doremus, R. W. Siegel, and R. Bizios, "Enhanced functions of osteoblasts on nanophase ceramics," *Biomaterials*, vol. 21, no. 17, pp. 1803–1810, 2000.

[11] J. Huang, S. M. Best, W. Bonfield et al., "In vitro assessment of the biological response to nano-sized hydroxyapatite," *Journal of Materials Science: Materials in Medicine*, vol. 15, no. 4, pp. 441–445, 2004.

[12] M. Okada, K. Furukawa, T. Serizawa et al., "Interfacial interactions between calcined hydroxyapatite nanocrystals and substrates," *Langmuir*, vol. 25, no. 11, pp. 6300–6306, 2009.

[13] S. Ramesh, C. Y. Tan, S. B. Bhaduri, W. D. Teng, and I. Sopyan, "Densification behaviour of nanocrystalline hydroxyapatite bioceramics," *Journal of Materials Processing Technology*, vol. 206, no. 1-3, pp. 221–230, 2008.

[14] L. Yang, B. W. Sheldon, and T. J. Webster, "Nanophase ceramics for improved drug delivery," *American Ceramic Society Bulletin*, vol. 89, no. 2, 2010.

[15] B. Ghiasi, Y. Sefidbakht, and M. Rezaei, "Hydroxyapatite for biomedicine and drug delivery," in *Nanomaterials for Advanced Biological Applications. Advanced Structured Materials*, M. Rahmandoust and M. Ayatollahi, Eds., vol. 104, pp. 85–120, Springer, Berlin, Germany, 2019.

[16] O. Geuli, N. Metoki, T. Zada, M. Reches, N. Eliaz, and D. S. Mandler, "Synthesis, coating, and drug-release of hydroxyapatite nanoparticles loaded with antibiotics," *Journal of Materials Chemistry B: Materials for Biology and Medicine*, vol. 5, no. 38, pp. 7819–7830, 2017.

[17] L. Zhao, W. Zhao, Y. Liu, X. Chen, and Y. Wang, "Nano-hydroxyapatite-derived drug and gene Co-delivery system for anti-angiogenesis therapy of breast cancer," *Medical Science Monitor*, vol. 23, pp. 4723–4732, 2017.

[18] T.-C. Coutinho, P.-W. Tardioli, and C.-S. Farinas, "Phytase immobilization on hydroxyapatite nanoparticles improves its properties for use in animal feed," *Applied Biochemistry and Biotechnology*, vol. 190, no. 1, pp. 270–292, 2020.

[19] Y. Lin, X. Wang, X. Huang, J. Zhang, N. Xia, and Q. Zhao, "Calcium phosphate nanoparticles as a new generation vaccine adjuvant," *Expert Review of Vaccines*, vol. 16, no. 9, pp. 895–906, 2017.

[20] Z. Shi, X. Huang, Y. Cai, R. Tang, and D. Yang, "Size effect of hydroxyapatite nanoparticles on proliferation and apoptosis of osteoblast-like cells," *Acta Biomaterialia*, vol. 5, no. 1, pp. 338–345, 2009.

[21] J. Jin, G. Zuo, G. Xiong et al., "The inhibition of lamellar hydroxyapatite and lamellar magnetic hydroxyapatite on the migration and adhesion of breast cancer cells," *Journal of Materials Science: Materials in Medicine*, vol. 25, no. 4, pp. 1025–1031, 2014.

[22] R. Meena, K.-K. Kesari, M. Rani, and R. Paulraj, "Effects of hydroxyapatite nanoparticles on proliferation and apoptosis of human breast cancer cells (MCF-7)," *Journal of Nano Research*, vol. 14, no. 2, p. 712, 2012.

[23] X. Chen, C. Deng, S. Tang, and M. Zhang, "Mitochondria-dependent apoptosis induced by nanoscale hydroxyapatite inhuman gastric cancer SGC-7901 cells," *Biological and Pharmaceutical Bulletin*, vol. 30, no. 1, pp. 128–132, 2007.

[24] J. Li, Y. Yin, F. Yao, L. Zhang, and K. Yao, "Effect of nano- and micro-hydroxyapatite/chitosan-gelatin network film on human gastric cancer cells," *Materials Letters*, vol. 62, no. 17-18, pp. 3220–3223, 2008.

[25] S. Dey, M. Das, and V.-K. Balla, "Effect of hydroxyapatite particle size, morphology and crystallinity on proliferation of colon cancer HCT116 cells," *Materials Science and Engineering: C*, vol. 39, pp. 336–339, 2014.

[26] S. Ezhaveni, R. Yuvakkumar, M. Rajkumar, N.-M. Sundaram, and V. Rajendran, "Preparation and characterization of nano-hydroxyapatite nanomaterials for liver cancer cell treatment," *Journal of Nanoscience and Nanotechnology*, vol. 13, no. 3, pp. 1631–1638, 2013.

[27] I.-W. Bauer, S.-P. Li, Y.-C. Han, L. Yuan, and M.-Z. Yin, "Internalization of hydroxyapatite nanoparticles in liver cancer cells," *Journal of Materials Science: Materials in Medicine*, vol. 19, no. 3, pp. 1091–1095, 2008.

[28] L. T. Wang, G. Zhou, H. F. Liu et al., "Nano-hydroxyapatite particles induce apoptosis on mc3t3-E1 cells and tissue cells in SD rats," *Nanoscale*, vol. 4, no. 9, pp. 2894–2899, 2012.

[29] B. Li, B. Guo, H. S. Fan, and X. D. Zhang, "Preparation of nano-hydroxyapatite particles with different morphology and their response to highly malignant melanoma cells in vitro," *Applied Surface Science*, vol. 255, no. 2, pp. 357–360, 2008.

[30] Y. Yuan, C.-S. Liu, J.-C. Qian, J. Wang, and Y. Zhang, "Size-mediated cytotoxicity and apoptosis of hydroxyapatite nanoparticles in human hepatoma HepG2 cells," *Biomaterials*, vol. 31, no. 4, pp. 730–740, 2010.

[31] M.-C. Wang, H.-T. Chen, W.-J. Shih, H.-F. Chang, M.-H. Hon, and I.-M. Hung, "Crystalline size, microstructure

and biocompatibility of hydroxyapatite nanopowders by hydrolysis of calcium hydrogen phosphate dehydrate (DCPD)," *Ceramics International*, vol. 41, no. 2, pp. 2999–3008, 2015.

[32] H. Jiang, J.-K. Liu, J.-D. Wang et al., "The biotoxicity of hydroxyapatite nanoparticles to the plant growth," *Journal of Hazardous Materials*, vol. 270, pp. 71–81, 2014.

[33] F. Vázquez-Hernández, S. Mendoza-Acevedo, C.-O. Mendoza-Barrera, J. Mendoza-Álvarez, and J.-P. Luna-Arias, "Antibody-coupled hydroxyapatite nanoparticles as efficient tools for labeling intracellular proteins," *Materials Science and Engineering: C*, vol. 71, pp. 909–918, 2017.

[34] M.-I. Domínguez, F. Romero-Sarria, M.-A. Centeno, and J.-A. Odriozola, "Gold/hydroxyapatite catalysts: synthesis, characterization and catalytic activity to CO oxidation," *Applied Catalysis B: Environmental*, vol. 87, no. 3-4, pp. 245–251, 2009.

[35] S. Lara-Ochoa, W. Ortega-Lara, and C. E. Guerrero-Beltrán, "Hydroxyapatite nanoparticles in drug delivery: physicochemistry and applications," *Pharmaceutics*, vol. 13, no. 10, p. 1642, 2021.

[36] T. G. P. Galindo, Y. Chai, and M. Tagaya, "Hydroxyapatite nanoparticle coating on polymer for constructing effective biointeractive interfaces," *Journal of Nanomaterials*, vol. 2019, Article ID 6495239, 23 pages, 2019.

[37] T. Leventouri, "Synthetic and biological hydroxyapatites: crystal structure questions," *Biomaterials*, vol. 27, no. 18, pp. 3339–3342, 2006.

[38] Y. Ryabenkova, N. Jadav, M. Conte et al., "Mechanism of hydrogen-bonded complex formation between ibuprofen and nanocrystalline hydroxyapatite," *Langmuir*, vol. 33, no. 12, pp. 2965–2976, 2017.

[39] A. Fahami, G. W. Beall, and T. S. Betancourt, "Synthesis, bioactivity and zeta potential investigations of chlorine and fluorine substituted hydroxyapatite," *Materials Science and Engineering: C*, vol. 59, pp. 78–85, 2016.

[40] K. Cheng, W. Weng, H. Wang, and S. Zhang, "In vitro behavior of osteoblast-like cells on fluoridated hydroxyapatite coatings," *Biomaterials*, vol. 26, no. 32, pp. 6288–6295, 2005.

[41] F. Wu, D. D. W. Lin, J. H. Chang, C. Fischbach, L. A. Estroff, and D. Gourdon, "Effect of the materials properties of hydroxyapatite nanoparticles on fibronectin deposition and conformation," *Crystal Growth & Design*, vol. 15, no. 5, pp. 2452–2460, 2015.

[42] Y. J. Tang, J. M. Ashcroft, D. Chen et al., "Charge-associated effects of fullerene derivatives on microbial structural integrity and central metabolism," *Nano Letters*, vol. 7, no. 3, pp. 754–760, 2007.

[43] L. Chen, J. M. Mccrate, J. C.-M. Lee, and H. Li, "The role of surface charge on the uptake and biocompatibility of hydroxyapatite nanoparticles with osteoblast cells," *Nanotechnology*, vol. 22, no. 10, Article ID 105708, 2011.

[44] S. Muthu Prabhu and S. Meenakshi, "Synthesis of surface coated hydroxyapatite powders for fluoride removal from aqueous solution," *Powder Technology*, vol. 268, pp. 306–315, 2014.

[45] H. Zhao, C. Wu, D. Gao et al., "Antitumor effect by hydroxyapatite nanospheres: activation of mitochondria-dependent apoptosis and negative regulation of phosphatidylinositol-3-kinase/protein kinase B pathway," *ACS Nano*, vol. 12, no. 8, pp. 7838–7854, 2018.

[46] G. Guo, A. Tian, X. Lan, C. Fu, Z. Yan, and C. Wang, "Nano hydroxyapatite induces glioma cell apoptosis by suppressing NF-κB signaling pathway," *Experimental and Therapeutic Medicine*, vol. 17, no. 5, pp. 4080–4088, 2019.

[47] X. Shi, K. Zhou, F. Huang, J. Zhang, and C. Wang, "Endocytic mechanisms and osteoinductive profile of hydroxyapatite nanoparticles in human umbilical cord wharton's jelly-derived mesenchymal stem cells," *International Journal of Nutrition*, vol. 13, pp. 1457–1470, 2018.

[48] X. Shi, K. Zhou, F. Huang, and C. Wang, "Interaction of hydroxyapatite nanoparticles with endothelial cells: internalization and inhibition of angiogenesis in vitro through the PI3K/akt pathway," *International Journal of Nutrition*, vol. 12, pp. 5781–5795, 2017.

[49] H. Zhang, F. Qing, H. Zhao, H. Fan, M. Liu, and X. Zhang, "Cellular internalization of rod- like nano hydroxyapatite particles and their size and dose-dependent effects on pre-osteoblasts," *Journal of Materials Chemistry B: Materials for Biology and Medicine*, vol. 5, no. 6, pp. 1205–1217, 2017.

[50] C. Y. Tay, W. Fang, M. I. Setyawati et al., "Nano-hydroxyapatite and nano-titanium dioxide exhibit different subcellular distribution and apoptotic profile in human oral epithelium," *ACS Applied Materials and Interfaces*, vol. 6, no. 9, pp. 6248–6256, 2014.

[51] X. Liu and J. Sun, "Potential proinflammatory effects of hydroxyapatite nanoparticles on endothelial cells in a monocyte–endothelial cell coculture model," *International Journal of Nutrition*, vol. 9, no. 1, pp. 1261–1273, 2014.

[52] C. S. Geetha, N. S. Remya, K. B. Leji et al., "Cells–Nano interactions and molecular toxicity after delayed hypersensitivity, in Guinea pigs on exposure to hydroxyapatite nanoparticles," *Colloids and Surfaces B: Biointerfaces*, vol. 112, pp. 204–212, 2013.

[53] C.-Y. Rao, X.-Y. Sun, and J.-M. Ouyang, "Effects of physical properties of nano-sized hydroxyapatite crystals on cellular toxicity in renal epithelial cells," *Materials Science and Engineering: C*, vol. 103, Article ID 109807, 2019.

[54] H. Turkez, M. I. Yousef, E. Sönmez et al., "Evaluation of cytotoxic, oxidative stress and genotoxic responses of hydroxyapatite nanoparticles on human blood cells," *Journal of Applied Toxicology*, vol. 34, no. 4, pp. 373–379, 2014.

[55] Z. Li, J. Tang, H. Wu et al., "A systematic assessment of hydroxyapatite nanoparticles used in the treatment of melanoma," *Nano Research*, vol. 13, no. 8, pp. 2106–2117, 2020.

[56] E. Obeng, "Apoptosis (programmed cell death) and its signals - a review," *Brazilian Journal of Biology*, vol. 81, no. 4, pp. 1133–1143, 2021.

[57] W. Tang, Y. Yuan, C. Liu, Y. Wu, X. Lu, and J. Qian, "Differential cytotoxicity and particle action of hydroxyapatite nanoparticles in human cancer cells," *Nanomedicine*, vol. 9, no. 3, pp. 397–412, 2014.